The Aeronautical Journal (2024), **128**, pp. 1729–1742
doi:10.1017/aer.2024.7

ROYAL AERONAUTICAL SOCIETY

RESEARCH ARTICLE

On the secondary stall of a wing in tandem configuration

S.H.R. Shah and A. Ahmed

Department of Aerospace Engineering, Auburn University, Auburn, AL 36849, USA
Corresponding author: S.H.R. Shah; Email: szs0196@auburn.edu

Received: 1 May 2023; **Revised:** 30 November 2023; **Accepted:** 9 January 2024

Keywords: tandem wings; low reynolds numbers aerodynamic; wing-vortex interaction; stall behaviour; post stall aerodynamics

Abstract

The aerodynamic response of a NACA0012 wing section was investigated at a Reynolds number of 100,000 in an open return wind tunnel in the presence of a second wing in tandem. The angle-of-attack of the front wing ranged from −5° to 90° while the rear wing remained at zero incidence. The presence of the downstream wing significantly altered the post-stall behaviour of the upstream wing in the form of a secondary stall characterised by a sudden drop in lift and drag for a specific combination of angle-of-attack and the spacing between the wings. The secondary stall was found to be insensitive to the Reynolds number and the aspect ratio of the downstream wing and did not affect the lift-to-drag ratio. Flow visualisation in the water tunnel indicated that the downstream wing effectively suppressed vortex shedding and lift fluctuations of the upstream wing.

Nomenclature

b	wing span
C_L	coefficient of lift, $C_L = L/0.5\rho V_\infty^2 S$
C_D	coefficient of drag, $C_D = D/0.5\rho V_\infty^2 S$
c	chord length
L/D	lift to drag ratio
Re	Reynolds number, $Re = \rho\, Vc/\mu$
s	streamwise spacing between wings
S	planform area of wing
AR	aspect ratio of wing
V_∞	freestream velocity

Greek symbol

α	angle-of-attack
ρ	density
μ	dynamic viscosity

1.0 Introduction

The aerodynamics of wings at low Reynolds number holds significant interest due to its relevance in various engineering applications for civil and military use such as the surveying and surveillance using RPVs (remotely piolted vehicles), MAVs (micro air vehicles), vehicles mimicking insect flights and perching birds, to name a few. The aerodynamic response of wings at low Reynolds numbers is sensitive to multiple factors such as the geometry, distribution of thickness and camber, taper and aspect

ratio [1–4]. Slightest disturbances in the freestream conditions lead to large changes in the aerodynamic response. In practice, a wing seldom operates in isolation or a disturbance-free environment. Examples include formation flight, wings, canards and elevators operating in the slipstream, vertical-axis wind turbines and rotors-stators interaction in turbomachinery. The aerodynamics of wings in the presence of various upstream disturbances such as gust encounters have far-reaching implications from the point of view of stability and performance degradation. The wake vortical interactions have been extensively explored in past research due to their importance while flying in close proximity, ground effect, and wake turbulence [5–10]. Most past studies investigating the aerodynamics of wing encounters with upstream wake disturbances have focused on the effects on downstream wings. Specifically, they have explored wings encountering wakes characterised by various vortical structures that differ in strength, orientation (both parallel and perpendicular), wavelength, frequency and length scales. These studies have analysed how such wake disturbances alter the aerodynamic response and performance of the downstream wing [4, 10–15]. However, there has been more limited investigation into the upstream effects of a rear wing on the aerodynamics of a forward wing and the wake interactions between them.

The aerodynamic response of rear wing depends on front wing, and at the same time, the presence of rear wing alters the wake of front wing. consequently, the wings are aerodynamically coupled, requiring simultaneous investigation. Scharpf and Muller [16] demonstrated that tandem wing configuration at low Reynolds numbers increased the range of Reynolds numbers for separated flow hysteresis, and downstream wing at a positive angle-of-attack caused a change in the pressure distribution around the upstream wing that resulted in reduced lift and drag. Shah and Ahmed [17] demonstrated that a downstream wing at a non-zero angle-of-attack deflects the wake of the upstream wing and hence induces a change in the effective angle-of-attack and both the wings stall together. Barnes et al. [11] reported the alteration in the path of the incident vortex due to the mutual induction between the incident vortex and tip vortex and the stronger interaction resulted in the rapid breakdown of the incident vortex into small-scale structures.

Low Reynolds number applications often operate at high angles of attack and often attain post-stall flight. Therefore, gaining a comprehensive understanding of the aerodynamic physical characteristics of wings in tandem configuration subject to unsteady loads under steady conditions necessitates a detailed analysis across the full range of angles of attack. This research experimentally investigates the aerodynamic response of a wing in the presence of a downstream wing of varying aspect ratios positioned at different streamwise locations in the wake. Wind tunnel testing and flow visualisation were utilised to study the aerodynamic response of the upstream wing due to wake modification and interference resulting from the downstream wing.

2.0 Experimental setup

Experiments were conducted in the open-return wind tunnel at Auburn University. The wind tunnel features a close test section that is 2.43 m long and has a cross-sectional area of 0.61 m × 0.61 m. The wind tunnel is equipped with a continuously variable frequency controller and can achieve a maximum velocity of 40 m/s. The turbulence level in the test section measured using a Dantec Dynamics 55P11 single-wire probe at the operating Reynolds number was less than 0.3%. Test models comprised two identical wings of NACA0012 sections, each with a chord length of 5.9 cm and a span of 35.2 cm. Wings with a rectangular planform area and rounded wing tips were made from aluminum on a CNC machine. The rounded wing tips prevented local flow separation at sharp edges and facilitated smoother flow in the tip region. The wings were installed in the test section in a cantilever arrangement. Therefore, the length of the wings represents the semi-span. The maximum blockage ratio of the wing at 90° was less than 6%, thus no blockage corrections were applied to the data presented. The velocity in the test section was calculated by employing a pitot-static tube with an error of less than 2%. A stepper motor attached to a 5:1 planetary gearbox was used to change the angle-of-attack statically, with a minimum resolution of 0.08°. A six-component force/moment balance (ATI Gamma sensor) was used to obtain force data.

https://doi.org/10.1017/aer.2024.7 Published online by Cambridge University Press

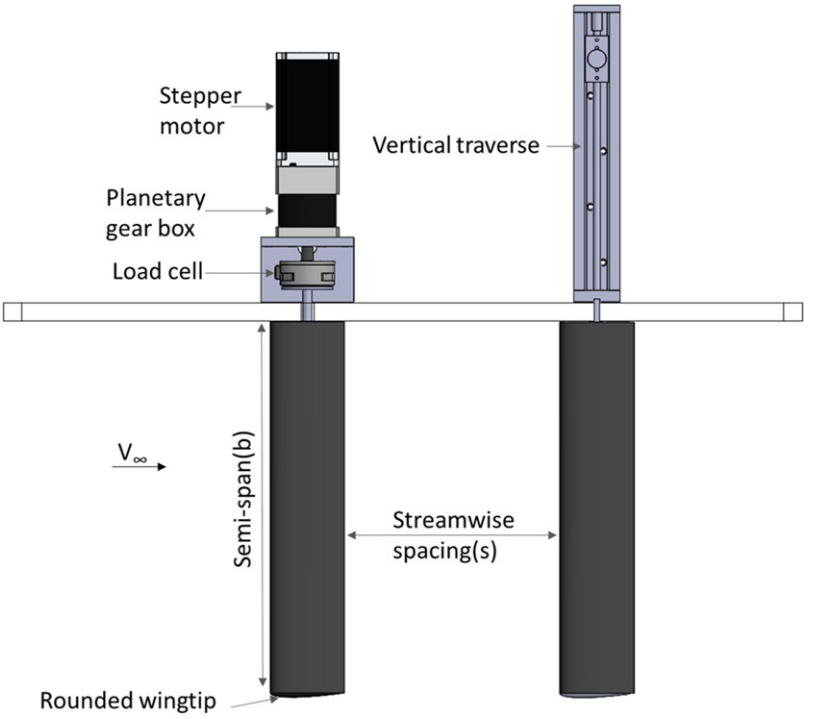

Figure 1. *Wind tunnel setup.*

The sensor has a range of 65 N in both the x and y-axes, with a resolution of 1/80 N. Meanwhile, the pitching axis aligned with the z-axis of the sensor had a resolution of 10/13333 Nm. For clarity, the upstream and downstream wings are denoted as Wing-1 and Wing-2, respectively. Wing-2 was attached to a vertical traverse mechanism to modify the aspect ratio by adjusting the span. Positioned within the wake of Wing-1, Wing-2 assumed various locations. The streamwise spacing or stagger(s) between the wings is defined as the distance between the trailing edge of Wing-1 and the leading edge of Wing-2, both set at 0° angle-of-attack. This distance was then varied across a range of 1 to 4 chord lengths. The schematic of the wind tunnel setup is shown in Fig. 1.

Wing-1 was attached to the sensor at the mid-chord hence the pitch axis is at the mid-chord, which allows Wing-2 to remain directly behind Wing-1. The sensor rotated with the wing to give normal (N) and axial (A) forces. Lift (L) and drag (D) were later obtained using simple transformation:

$$L = N\cos\alpha - A\sin\alpha \tag{1}$$

$$D = N\sin\alpha + A\cos\alpha \tag{2}$$

The angle-of-attack of Wing-2 was set at 0° while that of Wing-1 was varied from −5° to 90° in increments of 1°. To improve the readability of the plots, markers were placed at intervals of 2°. Data was sampled at 1 kHz, and for each angle-of-attack, the force signals were recorded for 10 s, resulting in 10,000 samples. This sampling duration and collected data was deemed sufficient to establish steady-state mean values. Additionally, a 4-s delay was introduced between incrementing the angle-of-attack and the start of data acquisition. Experiments were conducted at a chord-based Reynolds number of 100,000, corresponding to a velocity of 26.4 m/s. The precision limit of the force data was evaluated by examining the standard deviation and mean values for the isolated wing at each angle-of-attack, using a 95% confidence interval. The maximum uncertainty in C_L and C_D was approximately 7% and 5%,

https://doi.org/10.1017/aer.2024.7 Published online by Cambridge University Press

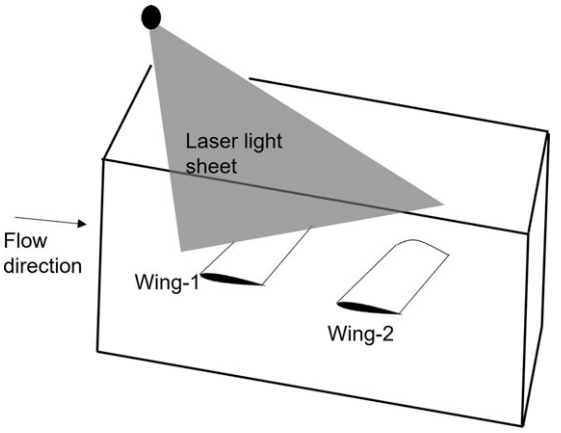

Figure 2. *Schematic of the flow visualisation setup in the water tunnel.*

respectively, at post-stall angles. In the pre-stall angle range, the uncertainty remained less than 3% and 2% for C_L and C_D, respectively.

Planar Laser Induced Fluorescence (PLIF) of sodium fluorescein was used for flow visualisation in the 46 cm × 46 cm cross-section closed loop water tunnel installed in the Vortex Dynamics Lab, Auburn University. Wing models of 10 cm chord and 40 cm span were mounted horizontally in a cantilevered arrangement. Wing-2 was attached to a horizontal traversing system to vary the streamwise spacing between the wings. A 5W CW Argon-Ion laser was utilised to illuminate the fluorescent dye in the mid-plane and wake of Wing-1. Videos were recorded at 60 fps and selected frames were later extracted to describe the flow features. Results were obtained for Wing-1 in isolation and later in tandem configuration for angles of attack of 15°, 25°, and 35°. Wing-2 was traversed horizontally to achieve wing spacing of $s = 1c$, $2c$, and $3c$. The schematic of the flow visualisation setup is shown in Fig. 2. Flow in the centre plane was considered quasi-symmetric or two-dimensional.

3.0 Results and discussion

Figure 3 shows the lift versus angle-of-attack of Wing-1 (AR = 6) in isolation at a Reynolds number of 100,000. The experimental results were compared with the data presented by Lind et al. [18] for a two-dimensional NACA0012 wing at a Reynolds number of 1.1×10^5, and Lee and Han [19] for NACA0012 wing of aspect ratio 6 at a Reynolds number of 1.0×10^5. The present data matches well in the pre-stall range of angle-of-attack, whereas the agreement of coefficient of lift in the post-stall and higher angles of attack is only qualitative and this discrepancy of data was attributed to the higher maximum blockage ratio and effects associated with their experimental setups which may result in exaggerated secondary peaks [20].

The results demonstrate that the lift curve slope for the isolated wing remained continuous over the entire range of the angles of attack, except at the stall angle (approximately 11°). In the pre-stall range, the lift curve exhibited a two-slope behaviour, which is well documented in the literature. At low Reynolds numbers, laminar boundary layer separation occurs before the natural transition to a turbulent boundary layer. Under certain conditions, the separated layer gets entrained from the freestream to reattach, forming a laminar separation bubble. As the angle-of-attack increases, this bubble moves toward the leading edge and decreases in size, causing the change in lift curve slope [21].

The data shows that lift continued to increase with the angle-of-attack until reaching the stall angle. The stall was abrupt and intense, characterised by a sharp peak, indicating a leading-edge stall caused by the sudden bursting of the separation bubble without subsequent reattachment. This stall behaviour is

https://doi.org/10.1017/aer.2024.7 Published online by Cambridge University Press

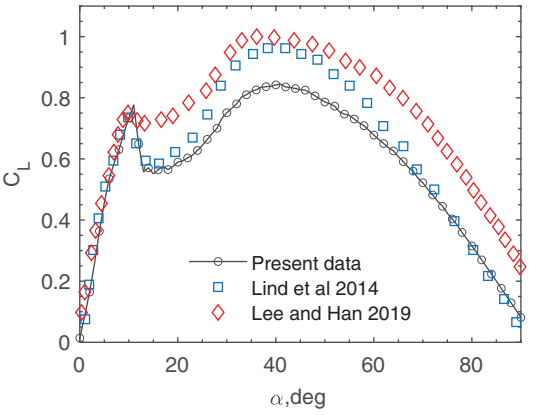

Figure 3. *C_L vs α of Wing-1 in isolation. AR = 6.*

commonly seen in moderately thick wings with thicknesses ranging from 9% to 15% [22]. Beyond the stall angle, lift gradually increased again with an increase in angle-of-attack, attaining a secondary peak at approximately 41°. This post-stall lift increase is attributed to the roll-up of separated shear layers resulting in significant vortical structures passing over the wing surface. After the secondary peak, the lift decreased in an almost linear fashion. Interestingly, the lift did not reach zero at 90°. This small amount of lift can be due to several factors, including wing deflection at high angles of attack due to the cantilever setup, suction at the rounded leading edge and the polar method of recording force and moment data, where the angle-of-attack was varied at a constant speed [23].

The present dataset conforms to the trends observed by various researchers [21, 24–26] in similar conditions, for both two-dimensional and three-dimensional NACA0012 wings. Therefore, the isolated wing data serves as the reference baseline in the present study. Any deviations in the results due to the presence of Wing-2 in the wake are attributed to aerodynamic interactions.

3.1 Secondary stall in tandem configuration and effect of streamwise spacing

Figures 4 and 5 show the time-averaged lift and drag versus the angle-of-attack of Wing-1 for the angle-of-attack range of −5° to 90° when Wing-2 was held at a constant incidence angle of 0° and positioned at downstream locations s = 1*c*–4*c*. The results are being compared with the isolated wing for reference. The findings highlight that the presence of Wing-2 had a negligible impact on the stall angle, mean lift and drag coefficients in the pre-stall angles of attack. However, a significant change in post-stall behaviour is evident, as illustrated in Figs. 4(b) and 5(b). The force data reveals a sudden reduction in aerodynamic forces at a critical angle-of-attack for each wing spacing. This abrupt decrease in both lift and drag at higher angles of attack is referred to as a 'secondary stall in tandem configuration'. This distinct secondary stall contrasts with the conventional primary stall, where the decrease in lift is accompanied by an increase in drag. Notably, the secondary stall was not abrupt for spacings of 1c, 1.5c and 4c, but it was pronounced for spacings of 2c to 3.5c. A notable drop of up to 15% in lift was recorded for a spacing of 2.5c. To the best of the knowledge of authors the phenomenon of a secondary stall occurring in tandem configuration has not been previously documented in the literature. However, Du et al. [27] observed a secondary stall for a single NACA0018 aerofoil tested in an open jet wind tunnel. Their analysis, employing surface flow visualisation, led them to infer that the expansion of the wake in an open jet tunnel facilitated the movement of the separation point from the suction side to the pressure side of the wing. This conclusion was substantiated when the same wing was tested in a closed jet wind tunnel, where the secondary stall did not manifest. Similarly, Worasinchai et al. [28] observed a secondary stall across four different aerofoils (NACA0012, SG6043, SD7062 and DU06-W-200) in a partially open test section where the wake could expand. The secondary stall was not observed

https://doi.org/10.1017/aer.2024.7 Published online by Cambridge University Press

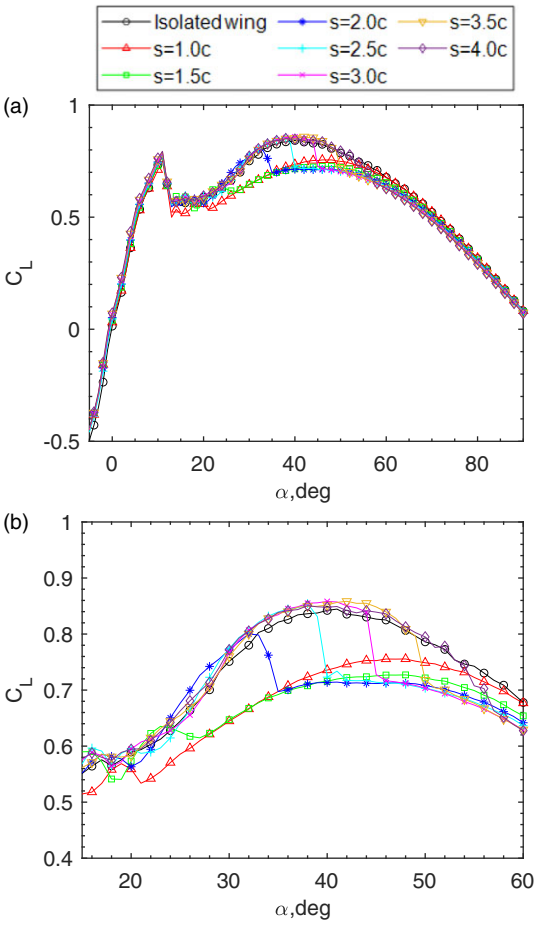

Figure 4. *C_L vs α of Wing-1 in tandem configuration.*

for isolated wings and aerofoils when aerodynamic coefficients were computed at low and very low Reynolds numbers, both computationally and experimentally [29, 30], in closed test section wind tunnels and water tunnels. It is important to mention that the present investigation was conducted in a closed test section wind tunnel, and the secondary stall for a single/isolated wing was not observed. However, the secondary stall only occurred when Wing-2 was positioned in the wake of Wing-1, i.e. in the tandem configuration. Consequently, it was inferred that aerodynamic interference due to Wing-2 was responsible for inducing the secondary stall. Lift-to-drag ratio is shown in Fig. 6. L/D ratio of approximately 12 was observed in the α range of 5° to 8°, and it sharply decreased at the stall, reaching zero linearly due to a simultaneous decrease in lift and an increase in drag at higher angles of attack. A slight increase in the maximum L/D was observed for tandem configurations. Interestingly, there was no effect of secondary stall on the lift-to-drag ratio. The variance in lift signal at each angle-of-attack was calculated and plotted as shown in Fig. 7. Variance represents the dispersion of the data and a smaller value of variance represents smaller fluctuations in the lift data. It was observed for the isolated wing the variance in the data increased at the stall angle and started to diminish gradually after approximately $\alpha = 41$ degrees. The secondary stall in tandem configurations resulted in a sudden drop of the C_L variance, however, for $s = 1$c the variance was less even for the pre-stall angles of attack.

https://doi.org/10.1017/aer.2024.7 Published online by Cambridge University Press

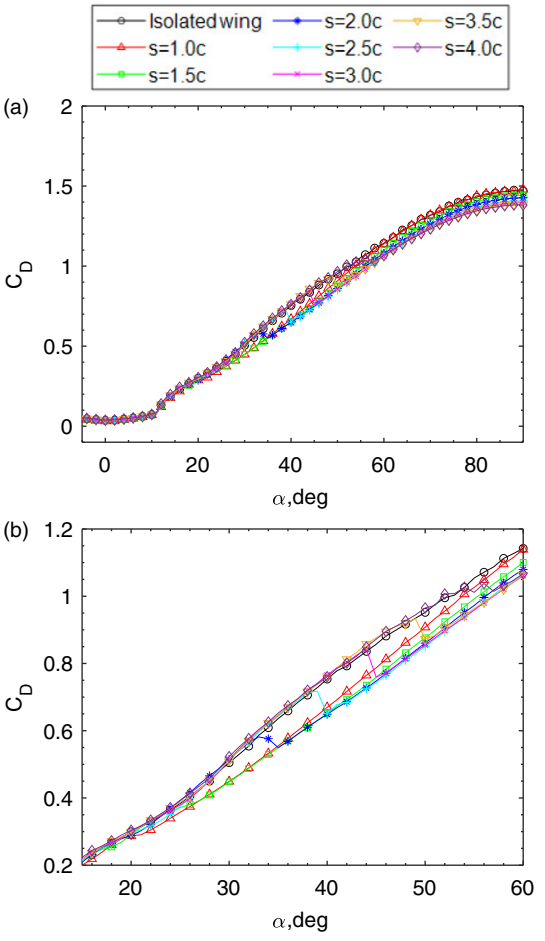

Figure 5. *C_D vs α of Wing-1 in tandem configuration.*

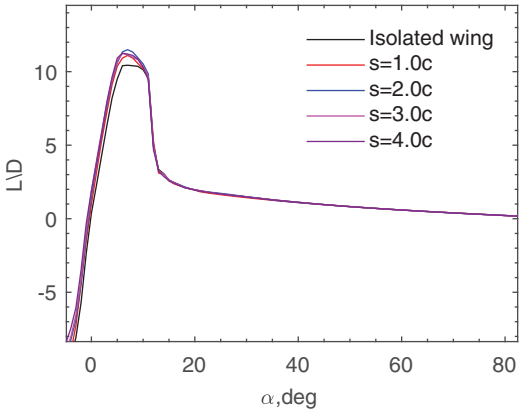

Figure 6. *Lift-to-drag ratio of Wing-1 in tandem configuration.*

https://doi.org/10.1017/aer.2024.7 Published online by Cambridge University Press

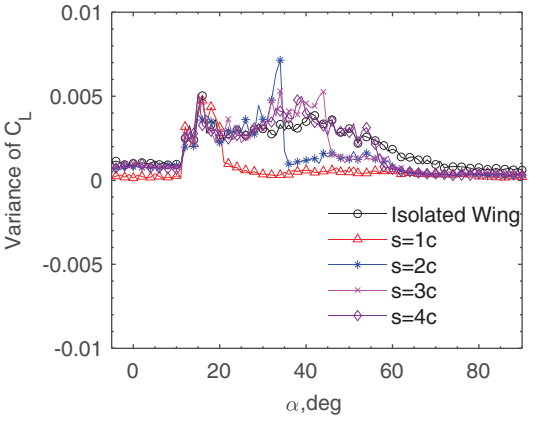

Figure 7. *Variance of C_L vs angle-of-attack of Wing-1 in tandem configuration.*

The critical angle-of-attack is defined as the angle-of-attack of Wing-1 at which the secondary stall occurs. The relationship between the critical angle-of-attack and streamwise spacing is shown in Fig. 8(a). The critical angle-of-attack and the spacing between the wings had an almost linear relation particularly for the $s = 2c$ to 4c as highlighted by the dotted line in Fig. 8(a). The projected distance of Wing-1 in the direction of flow was calculated using the sine relationship $csin(\alpha)$ and it was found that the secondary stall occurred whenever the distance between the leading edges of the Wing-1 and Wing-2 was around 18% of the streamwise projected distance of Wing-1 as shown in Fig. 8(b).

3.2 Secondary stall and three-dimensional behaviour of Wing-1

To investigate the effect of the span of Wing-1, two identical aspect ratio 4 wings of chord length 7.6 cm were utilised. Wings were made from PLA utilising 3D printing technology. Tests were carried out for the aspect ratio 4 wing in isolation, in tandem configuration ($s = 2c$), and by attaching a 17 cm round plate at the end to make it a two-dimensional wing. The lift vs angle-of-attack for the analysis utilising aspect ratio 4 wings in isolation and in tandem with and without end plate is shown in Fig. 9. The data was also compared with AR = 6 wings in tandem configuration. The results show that the secondary stall did not occur for AR = 4 wing when in tandem configuration, however lift values are slightly less for the angle-of-attack range of 35° to 60°. The addition of an endplate on Wing-1 resulted in an exaggerated second peak in the lift curve in isolation and the secondary stall in tandem configuration. This confirmed that the secondary stall phenomenon was due to the wake interaction of Wing-1. Furthermore, the tip vortices did not play any direct role in secondary stalls.

3.3 Effect of Reynolds number

The dependency of secondary stall on Reynolds number was investigated by varying the wind tunnel speed to achieve lower Reynolds numbers for $s = 2c$. While the anticipated effects of decreasing Reynolds numbers, such as earlier stall onset and alterations in C_{Lmax}, were evident, the secondary stall remained unaffected by the change in Reynolds number. Notably, the primary stall was not observable at the lowest Reynolds number tested, which was 20,000. The only stall evident corresponded to the secondary stall and stall was not apparent for the isolated wing at this Reynolds number as shown in Fig. 10(b). This observation leads to the inference that the secondary stall is primarily an inviscid phenomenon.

https://doi.org/10.1017/aer.2024.7 Published online by Cambridge University Press

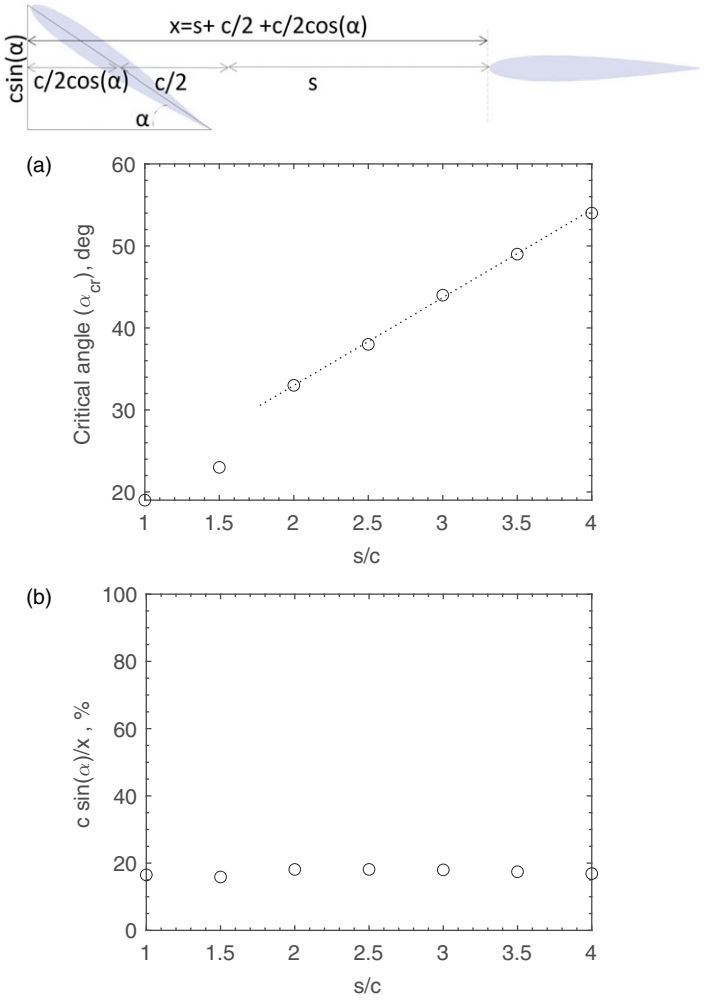

Figure 8. *Relationship between the wing projected thickness and wing spacing when secondary stall occurred.*

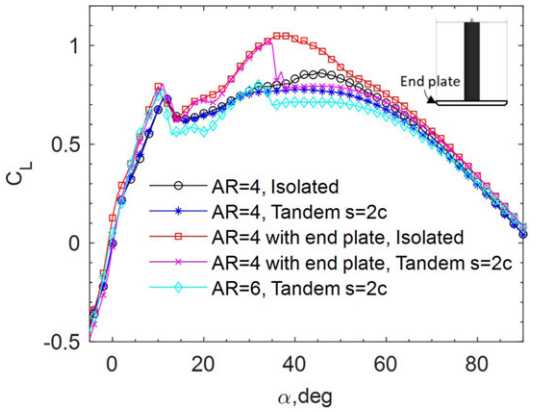

Figure 9. *Dependence of secondary stall on the aspect ratio of Wing-1.*

https://doi.org/10.1017/aer.2024.7 Published online by Cambridge University Press

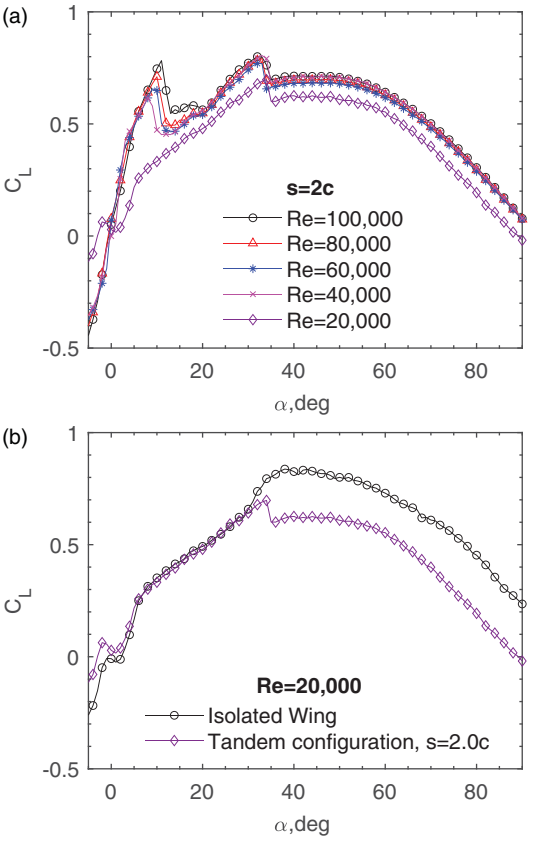

Figure 10. *Effect of Reynolds number on secondary stall.*

3.4 Effect of aspect ratio of Wing-2

In order to further investigate the dependence of the secondary stall, the span of Wing-2 was varied by using the vertical traverse. Testing was carried out by reducing the span to achieve aspect ratios of 4 and 2 for Wing-2. The results revealed that the behaviour of Wing-1 in the tandem configuration and the secondary stall were not affected by the changes in the span of the downstream wing as shown in Fig. 11.

3.5 Dye flow visualisation

Qualitative dye flow visualisation was carried out at three angles of attack of 15°, 25°, and 35° of Wing-1, and at a Reynolds number of 20,000 to understand the flow physics of the secondary stall as shown in Fig. 12. At all three angles, there was massive separation on the suction side starting from the leading edge with clearly visible reverse flow from the trailing edge towards the leading edge. Alternate vortex shedding from the shear layer of the separated boundary layer and the shear layer from the trailing edge. These vortices merge and form unstable Von Karman-type vortex streets with different vortical length scales [31]. The horizontal and vertical length scales of two connected counter-rotating vortices originating from the leading and trailing edges depend on angle-of-attack as observed for the isolated wing cases. The length scales grew larger with increasing angle-of-attack. The initiation location of the vortex pairs in the wake moved upstream towards the trailing edge as angle-of-attack increased [32]. For the tandem configurations, it was observed that the presence of Wing-2 prevented the two shear layers from interacting, depending on the angle-of-attack of Wing-1 and the spacing between the wings.

https://doi.org/10.1017/aer.2024.7 Published online by Cambridge University Press

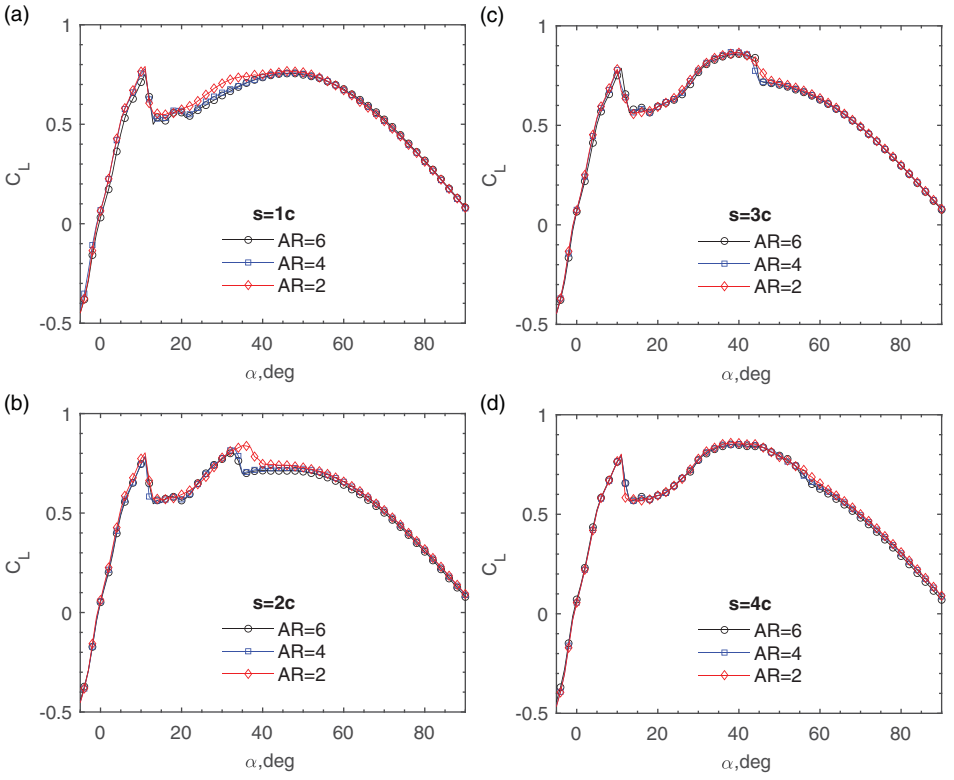

Figure 11. *Dependence of secondary stall on the aspect ratio of Wing-2.*

Alternate vortex shedding was observed at 25° for 2c and 3c spacing, and at 35° only for 3c spacing. Therefore, the combination of angle-of-attack and spacing results in two scenarios: a) alternate and periodic vortex formation between the wings. and b) suppression of vortex formation, with quasi-steady flow between the wings. In the periodic vortex case, the ability of Wing-1 to produce vortical lift at high angles and the drag produced was unaffected with respect to the isolated wing. However, when shear layers interaction became unattainable, the reverse flow observed from the leading edge of Wing-2 towards Wing-1 indicated the increase in static and higher adverse pressure gradient, consequently a reduction in aerodynamic forces lift and a decrease in life fluctuations. Therefore, it was inferred that at high angles, Wing-1 behaved like a bluff body and Wing-2 acted like a detached splitter plate [33, 34] and when positioned at a critical distance, it suppressed the vortex shedding from Wing-1 resulting in a sudden drop of lift and drag.

4.0 Conclusion

The secondary stall of an upstream wing (Wing-1) due to the presence of a downstream wing (Wing-2) in its wake was experimentally investigated in the wind tunnel and dye flow visualisation in the water tunnel. The results show that the secondary stall is an inviscid phenomenon and independent of the Reynolds number and was observed for two-dimensional wings and wings with higher aspect ratios ($\geq$ 5). Wing-2 acts like a detached splitter and at the critical combination of the angle-of-attack and spacing between the wings, it suppresses the vortex shedding from Wing-1 when two shear layers originating from the leading and trailing edges of Wing-1 cannot interact. As a consequence a sharp and sudden decrease in aerodynamic forces along with the reduction in lift fluctuation takes place.

https://doi.org/10.1017/aer.2024.7 Published online by Cambridge University Press

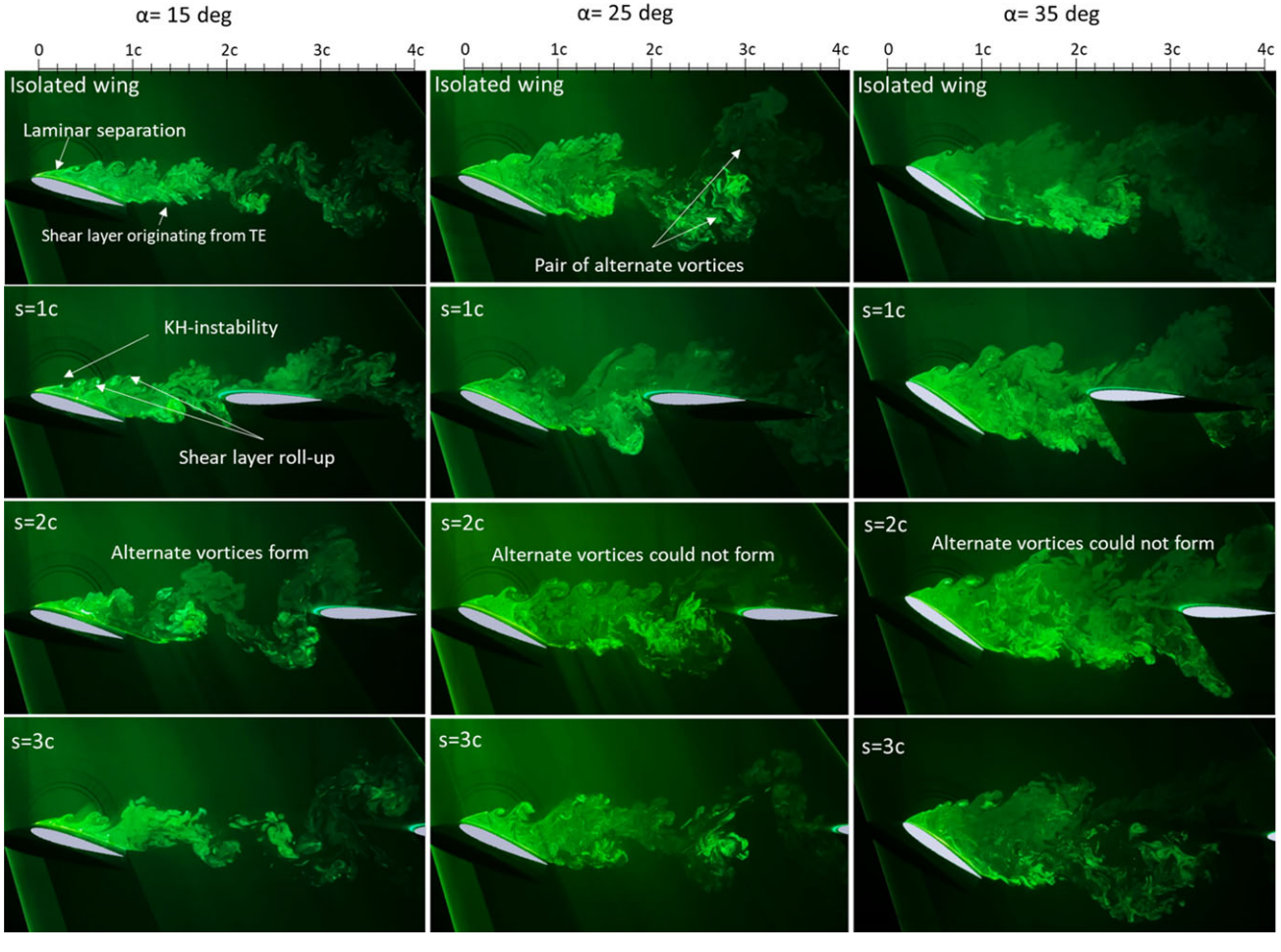

Figure 12. *Dye flow visualisation in isolation and tandem configuration.*

References

[1] McArthur, J. *Aerodynamics of wings at low Reynolds numbers: Boundary layer separation and reattachment*. PhD thesis, University of Southern California, 2008.

[2] Ananda, G.K., Sukumar, P.P. and Selig, M.S. Measured aerodynamic characteristics of wings at low Reynolds numbers, *Aerosp. Sci. Technol.*, 2015, **42**, pp 392–406. ISSN 1270-9638. https://doi.org/10.1016/j.ast.2014.11.016 https://www.sciencedirect.com/science/article/pii/S1270963814002612

[3] Torres, G.E. and Mueller, T.J. Low aspect ratio aerodynamics at low Reynolds numbers, *AIAA J.*, 2004, **42**, (5), pp 865–873. https://doi.org/10.2514/1.439

[4] Jones, A.R. and Cetiner, O. Overview of unsteady aerodynamic response of rigid wings in gust encounters, *AIAA J.*, 2021, **59**, (2), pp 731–736. https://doi.org/10.2514/1.J059602

[5] Bangash, Z.A., Sanchez, R.P., Ahmed, A. and Khan, M.J. Aerodynamics of formation flight, *J. Aircr.*, 2006, **43**, (4), pp 907–912. https://doi.org/10.2514/1.13872

[6] Yarusevych, S., Kawall, J.G. and Sullivan, P.E. Airfoil performance at low Reynolds numbers in the presence of periodic disturbances, *J. Fluids Eng.*, 2005, **128**, (3), pp 587–595. ISSN 0098-2202. https://doi.org/10.1115/1.2175165

[7] Mahalingam, R., Funk, R.B. and Komerath, N.M. Low speed canard-tip-vortex airfoil interaction, *SAE Trans.*, 1997, **106**, pp 136–143. ISSN 0096736X, 25771531. http://www.jstor.org/stable/44650388

[8] Davari, A.R., Doolabi, M.H., Soltani, M.R. and Izadkhah, M. Aspects of canard-wing vortices interaction in subsonic flow, *Sci. Iran.*, 2015, **22**, pp 743–754. https://api.semanticscholar.org/CorpusID:55014153

[9] Jones, R., Cleaver, D.J. and Gursul, I. Aerodynamics of biplane and tandem wings at low Reynolds numbers, *Exp. Fluids*, 2015, **56**, (6), p 124. ISSN 1432-1114. https://doi.org/10.1007/s00348-015-1998-3

[10] Vishnu, A., Babu, S., Medina, A., Rockwood, M., Bryant, M. and Gopalarathnam, A. Theoretical and experimental investigation of an unsteady airfoil in the presence of external flow disturbances, *J. Fluid Mech.*, 2021, **921**, p A21. ISSN 0022-1120. https://doi.org/10.1017/jfm.2021.484

[11] Barnes, C.J. and Visbal, M.R. Effects of vertical position and orientation on a vortical-gust/airfoil interaction at a transitional Reynolds number, In *47th AIAA Fluid Dynamics Conference*. https://arc.aiaa.org/doi/abs/10.2514/6.2017-3320

[12] Huang, R.F. and Lee, H.W. Effects of freestream turbulence on wing-surface flow and aerodynamic performance, *J. Aircr.*, 1999, **36**, (6), pp 965–972. https://doi.org/10.2514/2.2537

[13] Michelsen, W. and Mueller, T. Low Reynolds number airfoil performance subjected to wake interference from an upstream airfoil, In *5th Applied Aerodynamics Conference*. https://arc.aiaa.org/doi/abs/10.2514/6.1987-2351

[14] Khan, F.A. and Mueller, T.J. Tip vortex/airfoil interaction for a low Reynolds number canard/wingconfiguration, *J. Aircr.*, 1991, **28**, (3), pp 181–186. https://doi.org/10.2514/3.46010

[15] Turhan, B., Wang, Z. and Gursul, I. Interaction of vortex streets with a downstream wing, *Phys. Rev. Fluids*, 2022, **7**, (9), p 94701. https://link.aps.org/doi/10.1103/PhysRevFluids.7.094701

[16] Scharpf, D.F. and Mueller, T.J. Experimental study of a low Reynolds number tandem airfoil configuration, *J. Aircr.*, 1992, **29**, (2), pp 231–236. https://doi.org/10.2514/3.46149

[17] Hassan, S., Shah, R. and Ahmed, A. Experimental investigation of wings in tandem. In *AIAA AVIATION 2022 Forum*, **6**. https://arc.aiaa.org/doi/abs/10.2514/6.2022-3391

[18] Lind, A.H., Lefebvre, J.N. and Jones, A.R. Time-averaged aerodynamics of sharp and blunt trailing-edge static airfoils in reverse flow, *AIAA J.*, 2014, **52**, (12), pp 2751–2764. https://doi.org/10.2514/1.J052967

[19] Lee, S.H. and Han, Y.O. Experimental investigation of high-angle-of-attack aerodynamics of low-aspect-ratio rectangular wings configured with NACA0012 airfoil section, *Int. J. Aeronaut. Space Sci.*, **21**, (2), 2020, pp 303–314. ISSN 2093-2480. https://doi.org/10.1007/s42405-019-00215-z

[20] Traub, L.W. Effects of blockage on airfoils and wings at high angles of attack, *J. Aircr.*, 2015, **52**, (3), pp 990–993. https://doi.org/10.2514/1.C033119

[21] Winslow, J., Otsuka, H., Govindarajan, B. and Chopra, I. Basic understanding of airfoil characteristics at low Reynolds numbers (104–105), *J. Aircr.*, 2018, **55**, (3), pp 1050–1061. https://doi.org/10.2514/1.C034415

[22] Von Doenhoff, A.E. and Abbott, I.H. *Theory of Wing Sections: Including a Summary of Airfoil Data*.

[23] Mueller, T.J. and Brendel, M. *Preliminary experiments in unsteady flow on airfoils at low Reynolds numbers*.

[24] Mcghee, R.J., Walker, B.S. and Millard, B.F. Experimental results for the eppler 387 airfoil at low Reynolds numbers in the langley low-turbulence pressure tunnel, *Technical report*, National Aeronautics and Space Administration Scientific and Technical Information Division, Washington, DC, 1988.

[25] Kim, D.-H., Chang, J.-W. and Chung, J. Low-Reynolds-number effect on aerodynamic characteristics of a NACA 0012 airfoil. *J. Aircr.*, 2011, **48**, (4), pp 1212–1215. ISSN 0021-8669. https://doi.org/10.2514/1.C031223

[26] Ohtake, T., Nakae, Y. and Motohashi, T. Nonlinearity of the aerodynamic characteristics of NACA0012 aerofoil at low Reynolds numbers, *J. Jpn. Soc. Aeronaut. Space Sci.*, 2007, **55**, (644), pp 439–445. https://doi.org/10.2322/jjsass.55.439

[27] Du, L., Berson, A. and Dominy, R.G. Aerofoil behaviour at high angles of attack and at Reynolds numbers appropriate for small wind turbines, *Proc. Inst. Mech. Eng. C: J. Mech. Eng. Sci.*, 2015, **229**, (11), pp 2007–2022. https://doi.org/10.1177/0954406214550016

[28] Worasinchai, S., Ingram, G. and Dominy, R. A low-Reynolds-number, high-angle-of-attack investigation of wind turbine aerofoils, *Proc. Inst. Mech. Eng. A: J. Power Energy*, 2011, **225**, (6), pp 748–763. https://doi.org/10.1177/0957650911405411

[29] Alam, Md.M., Zhou, Y., Yang, H., Guo, H. and Mi, J. The ultra-low Reynolds number airfoil wake, *Exp. Fluids*, 2010, **48**, pp 81–103. https://api.semanticscholar.org/CorpusID:121445292

https://doi.org/10.1017/aer.2024.7 Published online by Cambridge University Press

[30] Kurtulus, D.F. On the unsteady behavior of the flow around NACA 0012 airfoil with steady external conditions at Re = 1000, *Int. J. Micro Air Veh.*, 2015, **7**, (3), pp 301–326. ISSN 1756-8293. https://doi.org/10.1260/1756-8293.7.3.301
[31] Temple, G. Collected works of Theodore von Karman, *J. Fluid Mech.*, 1959, **5**, (2), pp 329–336. ISSN 0022-1120. https://doi.org/10.1017/S0022112059210234
[32] Huang, R.F. and Lin, C.L. Vortex shedding and shear-layer instability of wing at low-Reynolds numbers, *AIAA J.*, 1995, **33**, (8), pp 1398–1403.
[33] Guan, G., He, K., Wang, P. and Yang, Q. Study on the parameters of detached splitter plate for VIV suppression, *Ocean Eng.*, 2022, **266**, p 113092. ISSN 0029-8018. https://doi.org/10.1016/j.oceaneng.2022.113092
[34] Hwang, J.-Y., Yang, K.-S. and Sun, S.-H. Reduction of flow-induced forces on a circular cylinder using a detached splitter plate, *Phys. Fluids*, 2003, **15**, (8), pp 2433–2436. ISSN 1070-6631. https://doi.org/10.1063/1.1583733

Cite this article: Shah S.H.R. and Ahmed A. (2024). On the secondary stall of a wing in tandem configuration. *The Aeronautical Journal*, **128**, 1729–1742. https://doi.org/10.1017/aer.2024.7